Multifunctionality and Control of the Crumpling and Unfolding of Large-Area Graphene

Jianfeng Zang[1], Seunghwa Ryu[2], Nicola Pugno[3], Qiming Wang[1], Qing Tu[1], Markus J. Buehler[2] Xuanhe Zhao[1*]

[1]Soft Active Materials Laboratory, Department of Mechanical Engineering and Materials Science, Duke University, USA
[2]Laboratory for Atomistic and Molecular Mechanics, Department of Civil and Environmental Engineering, Massachusetts Institute of Technology, USA
[3]Department of Civil, Environmental and Mechanical Engineering, Università di Trento, via Mesiano, 77 I-38123 Trento, Italy
*To whom correspondence should be addressed: xz69@duke.edu

Crumpled graphene films are broadly used, for instance in electronics[1], energy storage[2,3], composites[4,5], and biomedicine[6]. Although it is known that the degree of crumpling affects graphene's properties and the performance of graphene-based devices and materials[3,5,7], the controlled folding and unfolding of crumpled graphene films has not been demonstrated. Here we report an approach to reversibly control the crumpling and unfolding of large-area graphene sheets. We show with experiments, atomistic simulations and theory that, by harnessing the mechanical instabilities of graphene adhered on a biaxially pre-stretched polymer substrate and by controlling the relaxation of the pre-strains in a particular order, graphene films can be crumpled into tailored self-organized hierarchical structures that mimic superhydrophobic leaves. The approach enables us to fabricate large-area conductive coatings and electrodes showing superhydrophobicity, high transparency, and tunable wettability and transmittance. We also demonstrate that crumpled graphene-polymer laminates can be used as artificial-muscle actuators.

Graphene possess a unique combination[8] of extraordinary mechanical, electrical, thermal and optical properties and high specific surface area. Recent capability of synthesizing large-scale graphene[9,10] has motivated intensive efforts to integrate the merits of graphene into high-

performance devices and materials[1-6] ENREF 6. In these studies and applications, graphene films are generally wrinkled or rippled with smooth undulations[9,11,12] and/or crumpled with sharp ridges, folds and vertices[1-6,13]. Since deformation of graphene can strongly affect its properties and the performance of graphene-based devices and materials[3,5,7,14,15], it is highly desirable to control reversible wrinkling and crumpling of graphene. While it has been shown that thermal expansion and substrate regulation can induce reversible wrinkling of graphene[9,11,16,17] and capillary compression can crumple microscopic graphene flakes into particles[3,6], it is still not clear how to reversibly crumple and unfold large-area graphene films in a controlled manner. Such a capability, however, can potentially advance the performance of graphene-based devices and materials[3,5,7], as well as open avenues to exploit unprecedented properties of graphene. Here, we report a simple method to control reversible crumpling and unfolding of large-area graphene films, which yields novel conductive coatings and electrodes that are superhydrophobic, transparent, and feature tunable wettability and transmittance.

A film of few-layer graphene (3~10 layers) is grown on a nickel film by chemical vapor deposition and then transferred to a Polydimethylsiloxane (PDMS) stamp and characterized with Raman microscope (**Fig. S1** and **Fig. S2**)[9]. An elastomer film based on acrylic is biaxially stretched to 3~5 times of its original dimensions (*i.e.* pre-strained by 200%~400%) and held at the pre-stretched state. The graphene film is then transferred to the pre-stretched elastomer substrate by stamping[9]. Thereafter, the pre-strains in the substrate are relaxed sequentially along two pre-stretched directions as illustrated in **Fig. 1a**. During relaxation, the lateral dimensions of the transferred graphene film reduce macroscopically by the same ratio as those of the substrate. Microscopically, however, the graphene film develops wrinkles (**Fig. 1b**) and delaminated buckles (**Fig. 1c**) when the substrate is relaxed uniaxially, and become crumpled (**Fig. 1d**) when

the substrate is relaxed biaxially. If the relaxed substrate is biaxially stretched back, the crumpled graphene film can be unfolded to a relatively flat state (**Fig. 1e**). The crumpling-unfolding process is reversible over multiple cycles under the control of substrate deformation (**Fig. S3**). The method is also applicable to few-layer graphene grown on copper films (**Fig. S4**).

Now we discuss the underlying mechanisms that control the crumpling and unfolding of graphene through a joint experimental-theoretical-computational analysis. We first focus on the formation of wrinkles and delaminated buckles in graphene under uniaxial compression. As the pre-stretched substrate is gradually relaxed along one direction, the apparent length of the graphene film reduces from L_0 at initial (flat) state to L at current state (**Fig. 1a**). We define the macroscopic compressive strain in the graphene film along the relaxed direction as $\varepsilon_G = (L_0 - L)/L_0$. The compressive strain in graphene can be calculated as $\varepsilon_G = (\varepsilon_{pre} - \varepsilon)/(\varepsilon_{pre} + 1)$, where ε_{pre} is the pre-strain of the substrate and ε is the tensile strain in the substrate at current state. When the compressive strain in the graphene film reaches a critical value, wrinkles develop with an initial wavelength[11,18,19]

$$\lambda_0 = 2\pi h \left[\frac{E}{12\Lambda \mu_s (1-\upsilon^2)} \right]^{1/3} \tag{1}$$

where E and υ are the Young's modulus and Poisson's ratio of graphene, μ_s the shear modulus of the substrate taken to be a neo-Hookean material, h the thickness of the graphene film, and $\Lambda = \frac{1+(1+\varepsilon_{pre})^3}{2(1+\varepsilon_{pre})}$. Taking E = 1 TPa, $\upsilon = 0.165$, $\varepsilon_{pre} = 200\%$, and $\mu_s \approx 20$ kPa, we obtain $\lambda_0 \approx 611h$ [20]. Since the number of graphene layers ranges from 3 to 10, the initial wavelength is evaluated to be 0.6~2.1 μm, consistent with our experimental results (**Fig. 1b**)[11,19].

Under further uniaxial compression, a pattern of parallel ridges develops with wavelengths of 0.2~2 μm (**Fig. 1c** and **Fig. S5a**). By sectioning the graphene film (**Fig. S6**), we find that the ridges are due to buckling of delaminated regions of the graphene on substrate. The delaminated buckles may initiate from the hills of the wrinkles of graphene[21] and/or defects on the graphene-polymer interface[21-23]. Once initiated, the delaminated buckles will propagate until the decrease of the graphene-substrate system's elastic energy balances the increase of its interfacial energy[21-23]. Macroscopic and microscopic delaminations of films on compressed substrates have been extensively studied[21-23] and applied[24,25]. However, to our knowledge, the current study presents the first observation of patterns of delaminated buckles in large-area graphene films on polymer substrates, which is assessed using a close integration of experiment and atomistic simulation.

The crumpling of graphene films under biaxial compression leads to a surface structure that is distinct from the one formed under uniaxial compression. As discussed above, a pattern of parallel delaminated buckles form in graphene on the substrate when relaxed in one direction (**Fig. 1c** and **Fig. S5a**). As the substrate is subsequently relaxed in the other direction, the delaminated buckles are compressed along their ridges, and thus buckle and collapse (**Fig. 1d** and **Fig. S5b**). Furthermore, a new set of delaminated buckles develop perpendicular to the previous ones. The intersection of two orthogonal buckles gives rise to an interesting crumpling pattern with ridges and vertices (**Fig. 1d** and **Fig. S5b**). Our complementary atomistic simulation reveals high stress concentrations around the ridges and vertices, as shown in **Fig. 1f**. (Note that the feature size of the patterns from simulation is smaller than experimental observation because the simulation considers a single-layer graphene on a rigid surface, while the experiments are carried out with 3~10 layers of graphene on elastomer surface.) If the substrate is simultaneously

relaxed in the two directions, the crumpling also occurs but leads to more irregular patterns (**Fig. S7b** and **Fig. S8**). The difference in crumpling patterns generated by sequential versus simultaneous relaxations is also demonstrated by atomistic simulation (**Fig. S7**, **Movies S1** and **S2**). In addition, it is noted that the crumpling of delaminated graphene is distinct from the hierarchical folding of perfectly-bonded films under biaxial compression that was recently reported[26]. Once the relaxed substrate is biaxially stretched (to its initial length), the parts of graphene film adhered on the substrate will pull on the delaminated parts, unfolding the crumpled graphene film (**Fig. 1e, Fig. S3** and **Fig. S5c**). If the stretched substrate is relaxed again, the crumpling will reoccur. The graphene film can maintain its integrity over multiple crumpling-unfolding cycles (*i.e.* >50) with a few unconnected cracks emerging (**Fig. 1e** and **Fig. S3**).

The controlled crumpling of graphene leads to self-organized surface structures with controllable feature sizes ranging from nanometers to micrometers (**Fig. 1d** and **Fig. S5b**), and the hierarchical structure of crumpled graphene can be used for water-repellent and self-cleaning surfaces that mimic the structure of the lotus leaf, for example[27]. To demonstrate this effect we prepare a crumpled graphene film on a substrate with a biaxial pre-strain of 400%. As shown on **Fig. 2a**, a water drop placed on top of the crumpled graphene gives a static contact angle of $152°$. When the relaxed substrate is biaxially stretched back, the contact angle of the water drop is maintained above $150°$ until the biaxial tensile strain in the substrate exceeds 25% (**Fig. 2d**). If the substrate is further stretched, the contact angle of the water drop decreases as the crumpled graphene is unfolded (**Fig. 2d** and **Fig. S3**). Once the graphene is fully unfolded, the contact angle of the water drop decreases to $105°$ (**Fig. 2b**), approximately the same as that of a water drop on a bare substrate (**Fig. 2c**) due to the wetting transparency of graphene[28]. Therefore, one

can instantaneously tune the wettability of large-area surfaces by simply stretching substrates coated with crumpled graphene, which does not require a complicated fabrication approach[29].

The tunable wettability of crumpled graphene can also be achieved by stretching substrates with different levels of biaxial pre-strains (*i.e.* 250% and 100% in **Fig. 2d**). If the water contact angle is re-plotted as functions of the compressive strain in graphene, the curves for different pre-strains collapse on a universal curve (**Fig. 2e**). We use the Wenzel and Cassie-Baxter models to explain the water contact angle on crumpled graphene ENREF 33. When the graphene is flat or slightly crumpled, the water will be in conformal contact with the graphene on substrate (*i.e.* Wenzel state in **Fig. 2e**). In addition, the water will feel the wettability of polymer substrate due to wetting transparency of graphene[28]. On the other hand, if the graphene is highly crumpled, the water drop will sit on a composite of graphene and air (*i.e.* Cassie-Baxter state in **Fig. 2e**) and the graphene-air composite is no longer transparent to wetting. Therefore, the apparent contact angle θ of the water drop can be calculated as

$$\cos\theta = r\cos\theta_0^S \qquad \text{(at Wenzel state)} \tag{2a}$$

$$\cos\theta = r\left(1-f_a\right)\cos\theta_0^G - f_a \qquad \text{(at Cassie-Baxter state)} \tag{2b}$$

where $\theta_0^S = 105°$ and $\theta_0^G = 90.6°$ are the water contact angle on polymer substrate and graphite respectively, f_a the air fraction in the contact area at Cassie-Baxter state, and r the roughness of the wetted surface area. The roughness can be calculated by $r = 1/\left(1+d\varepsilon_G\right)^2$, where $0 < d \le 1$ takes into account the observed delamination, giving the portion of compressive strain in graphene that contributes to the roughness. With $d = 0.82$ and $f_a = 0.61$, our model matches the experimental data very well (**Fig. 2e**).

The crumpled graphene films can also be used as extremely stretchable and transparent electrodes. To enhance the transparency of crumpled graphene, we pre-stretch the substrate in two directions by unequal pre-strains of 10% and 500%. Thereafter, the relaxed substrate is uniaxially stretched along the direction with higher pre-strain, while the resistance of the graphene film is measured. The crumpled graphene electrode can maintain good conductivity when the substrate is repeatedly stretched to an extremely high strain of 450% or highly twisted to an angle of 360° (**Fig. 3a** and **b**). On the other hand, under the same deformations (*i.e.* stretching or twisting), a crumpled gold film of 20 nm thick develops long and connected cracks with its resistance irreversibly increased by orders of magnitude (**Fig. S9**). The graphene film only begins to fracture significantly when the tensile strain of the substrate exceeds its pre-strain (**Fig. S10**). These results support that graphene film can maintain its integrity over multiple crumpling-unfolding cycles, owing to its high toughness and deformability[20]. Furthermore, when the substrate is stretched, the transmittance of the electrode in visible range increases from 30% to 80% as the crumpled graphene is being unfolded (**Fig. 3c**). The contact angle of a water drop on the graphene electrode can also be varied from 135° to 103° as shown in **Fig. 3d** by stretching the substrate. (Note that our contact angle model is still valid here, considering $r = 1/\left[\left(1+d\varepsilon_{G1}\right)\left(1+d\varepsilon_{G2}\right)\right]$, where ε_{G1} and ε_{G2} are compressive strains in graphene along two directions.) The water-repellent capability of the crumpled-graphene electrode can be further enhanced by increasing biaxial pre-strains of the substrate (e.g. **Fig. 2a**). To our knowledge, this combination of stretchability, transparency, and tunability has not been achieved by existing graphene electrodes[9] or other flexible electrodes based on metal films, conductive polymers, indium tin oxide, nanowires or carbon nanotubes. These properties make crumpled graphene electrodes particularly suitable for niche applications such as actuators and energy harvesters[30].

Here we demonstrate the application of a laminate of crumpled graphene and dielectric elastomer as a novel artificial-muscle actuator[30]. We biaxially pre-stretch a dielectric-elastomer film by equal pre-strains of 450%, transfer graphene films on its top and bottom surfaces, and then relax the elastomer film to a lower biaxial tensile strain of 300%. As a direct-current voltage of 3,000 V is applied between the graphene films, the elastomer develops an electric field that induces the Maxwell stress[30]. The Maxwell stress deforms the laminate by reducing its thickness and increasing its area over 100% (**Movie S3** and **Fig. 4a).** The actuation is fast and the graphene-elastomer laminate restores its undeformed state once the voltage is withdrawn. The transmittance of the laminate varies between 40% and 60% during actuation (**Fig. 4b**), yielding an artificial muscle with tunable transparency. It is noted that the partial delamination of the graphene film from the substrate is critical to the function of the graphene electrode, where the delaminated part of the graphene enables its high stretchability while the attached part ensures its macroscopically conformal deformation with the elastomer. In contrast, a graphene-elastomer laminate with flat non-delaminated graphene electrodes can only achieve an area strain of 20% in the first actuation and 7.6% in the second actuation due to fracture of the flat graphene electrodes (**Fig. S11**)[9].

In summary, here we demonstrated a simple method to reversibly crumple and unfold large-area graphene, which enables us to achieve a set of unprecedented morphologies and properties of graphene, in a controlled manner. A number of future research directions become possible, such as systematic and quantitative investigations of the effects of crumpling on graphene's electrical and electrochemical properties[1-3] and the strengths of graphene-polymer interfaces[4,5]. In addition, the ridges and vertices in the crumpled graphene are highly deformed and microscopically patterned, which can potentially lead to other new properties and

applications of graphene, such as patterned chemical reactions[31] or for applications in biomedical devices. Furthermore, by controlling the microscopic patterns of graphene with a simple macroscopic tool, one can develop new graphene-based systems with novel tunablility and flexibility to make nanoscale mechanisms visible at the macroscale.

Methods

Preparation of crumpled graphene. Few-layer graphene films grown on nickel films on silicon wafers with chemical vapor deposition are purchased from Graphene Supermarket (USA) and used as received. A PDMS stamp is adhered to the graphene film on the wafer (**Fig. S1**) [9]. The graphene film with the PDMS stamp is detached from the wafer by etching off the nickel film in 1 M $FeCl_3$ solution. The graphene/PDMS sample is rinsed by isopropanol and deionized water and dried in air or nitrogen gas. The cleaned graphene/PDMS sample is stamped on a biaxially pre-stretched (with pre-strain of 200%~400%) elastomer film of VHB acrylic 4905 (3M, USA) to transfer the graphene film to the elastomer film. Thereafter, the pre-strains in the substrate are relaxed sequentially along two pre-stretched directions. The whole process is schematically illustrated in Step I of **Fig. S1**.

Characterization of microscopic patterns of graphene on elastomer substrates. Scanning electron microscope (SEM, FEI XL30 SEM-FEG, USA) and atomic force microscope (AFM, Digital Instrumentas dimension 3100, Bruker, Germany) in tapping mode are employed to characterize the morphologies of various patterns on graphene films including wrinkles, delaminated buckles, crumples, and unfolded crumples.

Measurement of water contact angle. A water drop of 1~3 μ L is placed on the surface of the graphene and images are immediately captured for static contact angle measurements using a

side-view microscope connected with a camera (Nikon, USA). The water drops are removed by compressive air to dry the graphene surface for repeated contact angle experiments. The contact angle is measured using image processing software, ImageJ.

Transmittance measurement. The transmittance of graphene electrodes on elastomer films are measured using a UV/VIS spectrometer (Cary 6000i, USA) at a wavelength of 550 nm in visible range.

Voltage-induced actuation of graphene-elastomer laminate. Graphene films are transferred to the top and bottom surfaces of a biaxially pre-stretched elastomer film by stamping (**Fig. S1**). The pre-stretches in the elastomer film are relaxed sequentially along two pre-stretched directions to a lower pre-strain. A high voltage supply (Matsusada, Japan) with controllable ramping rate is used to apply a high voltage between the top and bottom graphene electrodes. The voltage is ramped up to 3000 V in 0.05 S and then reduced to 0V.

Atomistic simulation of crumpling of graphene. We model the crumpling of a single layer of graphene spanning 100 nm by 100 nm (383,125 atoms), confined on a rigid surface. The Adaptive Intermolecular Reactive Empirical Bond Order (AIREBO) potential for carbon[32] is used for full-atomistic Molecular Dynamics (MD) simulations. Van der Waals interactions between the graphene film and the substrate are modeled by a Lennard-Jones 9:3 wall potential corresponding to an adhesive energy of 100 mJ/m^2 and equilibrium distance of d = 3.35 Å. All MD simulations are performed using LAMMPS[33] with a time step of 3 fs. Periodic boundary conditions (PBC) are applied to the two orthogonal directions parallel to the wall surface. Before loading the graphene film in compression, it is equilibrated for 30 ps in the *NVT* ensemble using a Langevin thermostat at 300 K. After equilibration, the equibiaxial compression simulation is

performed using the Nose-Hoover thermostat in which the graphene film is scaled down in both *x*- and *y*-directions by -0.5% of the initial length at every 10 ps until the strain reaches -50%, corresponding to a strain rate of 10^8 s^{-1}. The sequential compression simulation is performed with identical condition but at a twice faster strain rate along each axis, *i.e.* 2×10^8 s^{-1}, to ensure that the total compression time is identical to that of the equibiaxial simulation. The strain rate is chosen such that the observed crumpling pattern has a smaller characteristic scale as the simulation cell size. Because of the finite substrate modulus and thicker graphene film, the overall scale of crumpled morphology cannot be compared directly with experiments, but our simulation results capture the fundamental mechanism and structures of graphene crumpling for the two distinct compression paths.

Acknowledgements

The research is primarily funded by the NSF's Research Triangle MRSEC (DMR-1121107), NSF (CMMI-1200515) and NIH (UH2 TR000505). X.Z. acknowledges the support from Pratt School of Engineering Seed Grant. S.R. and M.J.B acknowledge the support from AFOSR (FA9550-11-1-0199) and NSF-MRSEC (DMR-0819762). M.J.B. and N.M.P. acknowledge the support from the MIT-Italy Program (MITOR). N.M.P. acknowledges the support from the European Research Council under the European Union's Seventh Framework Programme (FP7/2007–2013)/ERC Grant agreement nu [279985] (ERC StG Ideas 2011 BIHSNAM). J.Z. and X.Z. acknowledge the help from Chuan-Hua Chen on contact angle measurement and Benjamin Wiley on transmittance measurement.

Author contributions

X.Z. conceived the idea, designed and supervised the experiments, and performed the data interpretation. J.Z. designed and carried out the experiments, and performed the data interpretation. Q.W. and Q.T. supported the experiments and contributed to the data interpretation. S.R. and M.J.B. designed, carried out, analyzed and interpreted the atomistic simulations. N.P., S.R., M.J.B., and X.Z. developed the theoretical models and interpreted them. X.Z. drafted the manuscript and all authors contributed to the writing of the manuscript.

Additional information

The authors declare no competing financial interests. Supplementary information accompanies this paper on www.nature.com/naturematerials. Reprints and permissions information is available online at www.nature.com/reprints. Correspondence and requests for materials should be addressed to X.Z. (xz69@duke.edu).

References

1 Miller, J. R., Outlaw, R. A. & Holloway, B. C. Graphene double-layer capacitor with ac line-filtering performance. *Science* **329**, 1637-1639, (2010).

2 Zhu, Y. *et al.* Carbon-based supercapacitors produced by activation of graphene. *Science* **332**, 1537-1541, (2011).

3 Luo, J. *et al.* Compression and aggregation-resistant particles of crumpled soft sheets. *Acs Nano* **5**, 8943-8949, (2011).

4 Stankovich, S. *et al.* Graphene-based composite materials. *Nature* **442**, 282-286, (2006).

5 Ramanathan, T. *et al.* Functionalized graphene sheets for polymer nanocomposites. *Nature Nanotechnology* **3**, 327-331, (2008).

6 Chen, Y. *et al.* Aerosol synthesis of cargo-filled graphene nanosacks. *Nano Letters* **12**, 1996-2002 (2012).

7 Pereira, V. M., Castro Neto, A. H., Liang, H. Y. & Mahadevan, L. Geometry, mechanics, and electronics of singular structures and wrinkles in graphene. *Physical Review Letters* **105**, 156603, (2010).

8 Geim, A. K. & Novoselov, K. S. The rise of graphene. *Nature Materials* **6**, 183-191, (2007).

9 Kim, K. S. *et al.* Large-scale pattern growth of graphene films for stretchable transparent electrodes. *Nature* **457**, 706-710, (2009).

10 Li, X. *et al.* Large-area synthesis of high-quality and uniform graphene films on copper foils. *Science* **324**, 1312-1314, (2009).

11 Bao, W. *et al.* Controlled ripple texturing of suspended graphene and ultrathin graphite membranes. *Nature Nanotechnology* **4**, 562-566, (2009).

12 Meyer, J. C. *et al.* The structure of suspended graphene sheets. *Nature* **446**, 60-63, (2007).

13 Cranford, S. W. & Buehler, M. J. Packing efficiency and accessible surface area of crumpled graphene. *Physical Review B* **84**, 205451, (2011).

14 Levy, N. *et al.* Strain-induced pseudo-magnetic fields greater than 300 Tesla in graphene nanobubbles. *Science* **329**, 544-547, (2010).

15 Guinea, F., Katsnelson, M. I. & Geim, A. K. Energy gaps and a zero-field quantum Hall effect in graphene by strain engineering. *Nature Physics* **6**, 30-33, (2010).

16 Scharfenberg, S. *et al.* Probing the mechanical properties of graphene using a corrugated elastic substrate. *Applied Physics Letters* **98**, 091908, (2011).

17 Li, T. & Zhang, Z. Substrate-regulated morphology of graphene. *Journal of Physics D-Applied Physics* **43**, 075303, (2010).

18 Cao, Y. & Hutchinson, J. W. Wrinkling phenomena in neo-Hookean film/substrate bilayers. *Journal of applied Mechanics* **79**, 031019 (2012).

19 Wang, Y. *et al.* Super-elastic graphene ripples for flexible strain sensors. *Acs Nano* **5**, 3645-3650, (2011).

20 Lee, C., Wei, X., Kysar, J. W. & Hone, J. Measurement of the elastic properties and intrinsic strength of monolayer graphene. *Science* **321**, 385-388, (2008).

21 Mei, H., Landis, C. M. & Huang, R. Concomitant wrinkling and buckle-delamination of elastic thin films on compliant substrates. *Mechanics of Materials* **43**, 627-642, (2011).

22 Hutchinson, J. W. & Suo, Z. Mixed-mode cracking in layered materials. *Advances in Applied Mechanics* **29**, 63-191, (1992).

23 Vella, D., Bico, J., Boudaoud, A., Roman, B. & Reis, P. M. The macroscopic delamination of thin films from elastic substrates. *Proceedings of the National Academy of Sciences of the United States of America* **106**, 10901-10906, (2009).

24 Rogers, J. A., Someya, T. & Huang, Y. Materials and mechanics for stretchable electronics. *Science* **327**, 1603-1607, (2010).

25 Kaltenbrunner, M. *et al.* Ultrathin and lightweight organic solar cells with high flexibility. *Nature Communications* **3**, 770, (2012).
26 Kim, P., Abkarian, M. & Stone, H. A. Hierarchical folding of elastic membranes under biaxial compressive stress. *Nature Materials* **10**, 952-957, (2011).
27 Neinhuis, C. & Barthlott, W. Characterization and distribution of water-repellent, self-cleaning plant surfaces. *Annals of Botany* **79**, 667-677, (1997).
28 Rafiee, J. *et al.* Wetting transparency of graphene. *Nature Materials* **11**, 217-222, (2012).
29 Zhang, Z., Zhang, T., Zhang, Y. W., Kim, K.-S. & Gao, H. Strain-Controlled Switching of Hierarchically Wrinkled Surfaces between Superhydrophobicity and Superhydrophilicity. *Langmuir* **28**, 2753-2760, (2012).
30 Pelrine, R., Kornbluh, R., Pei, Q. B. & Joseph, J. High-speed electrically actuated elastomers with strain greater than 100%. *Science* **287**, 836-839, (2000).
31 Ruoff, R. A means to an end. *Nature* **483**, S42-S42, (2012).
32 Stuart, S. J., Tutein, A. B. & Harrison, J. A. A reactive potential for hydrocarbons with intermolecular interactions. *Journal of Chemical Physics* **112**, 6472-6486, (2000).
33 Plimpton, S. Fast parallel algorithms for short-range molecular-dynamics. *Journal of Computational Physics* **117**, 1-19, (1995).

Figure captions

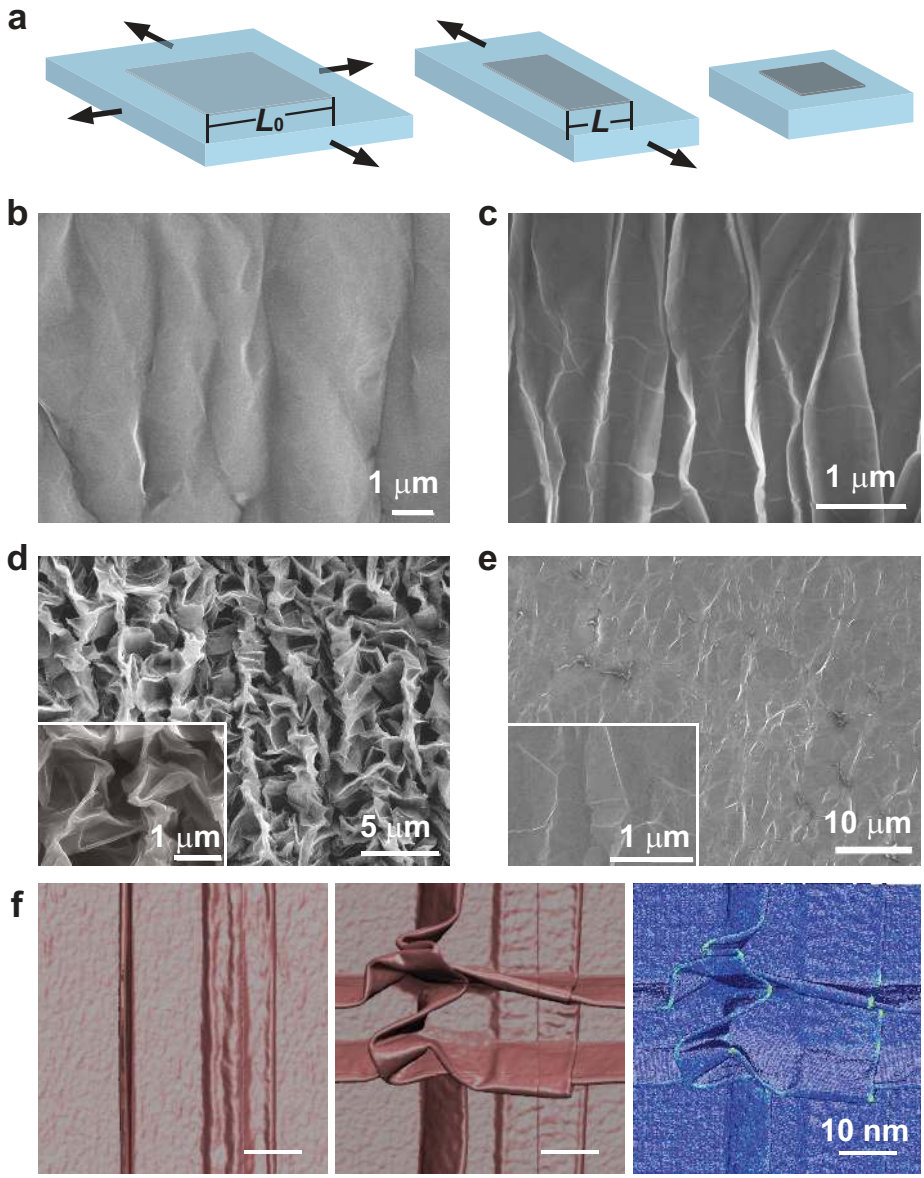

Fig 1. Controlled crumpling and unfolding of large-area graphene sheets. a, Schematic illustration of macroscopic deformation of a graphene sheet on a biaxially pre-stretched substrate. **b-d,** SEM images of patterns developed on the graphene sheet: **b,** wrinkles and then **c,** delaminated buckles as the substrate is uniaxially relaxed, **d,** crumples as the substrate is biaxially relaxed, and **e,** crumples unfolded as the substrate is biaxially stretched back. **f,** Atomistic modeling results of the crumpling of a single layer graphene under uniaxial

compression, and biaxial compression, followed by a visualization of the Mises stress distribution (from left to right). Stress concentrations (visualized in red) are observed near highly deformed regions.

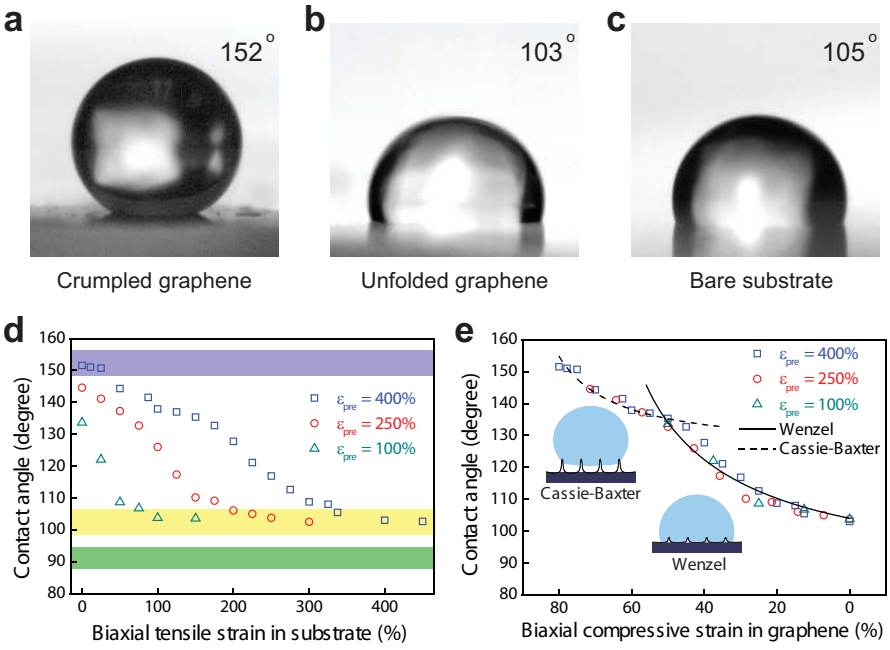

Fig 2. Stretchable graphene coatings capable of superhydrophobicity and tunable wettability. a-c, Image showing the contact angle of a water drop: **a,** 152° on highly crumpled graphene, **b,** 103° on unfolded graphene, and **c,** 105° on bare substrate. **d,** Contact angle as a function of the biaxial tensile strain in the substrate, ε, with various levels of pre-strain. The contact angle of a water drop on unfolded graphene is closer to that on a bare substrate (yellow band) than that on graphite (green band). **e,** Contact angle as a function of biaxial compressive strain in graphene, ε_G. The experimental results can be explained by our theoretical model. Values in **d** and **e** represent mean of n tests (n = 3-5).

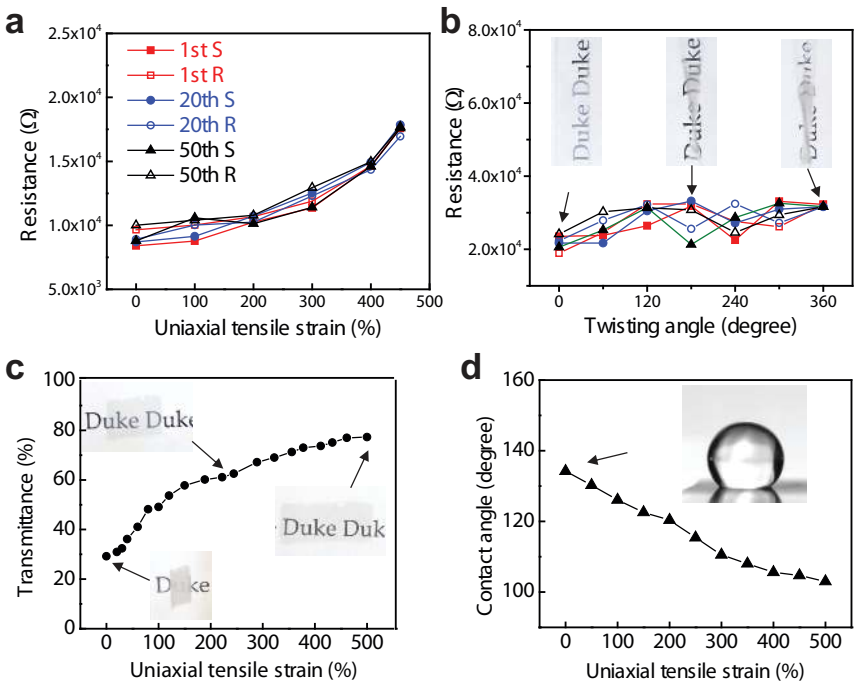

Fig 3. Graphene electrodes capable of giant stretchability and tunable transparency and wettability. a, Resistance of the electrode on a substrate under multiple cycles of uniaxial tensile strain up to 450%, and **b,** twisting up to 360°. The inset shows the electrode under twisting. **c,** Transmittance of the electrode in visible range as a function of uniaxial strain in the substrate. The insect shows the electrode under tension. **d,** Contact angle of a water drop on the electrode as a function of uniaxial strain in the substrate. The inset shows a water drop on the electrode on an undeformed substrate. Values represent mean of *n* tests (*n* = 3-5).

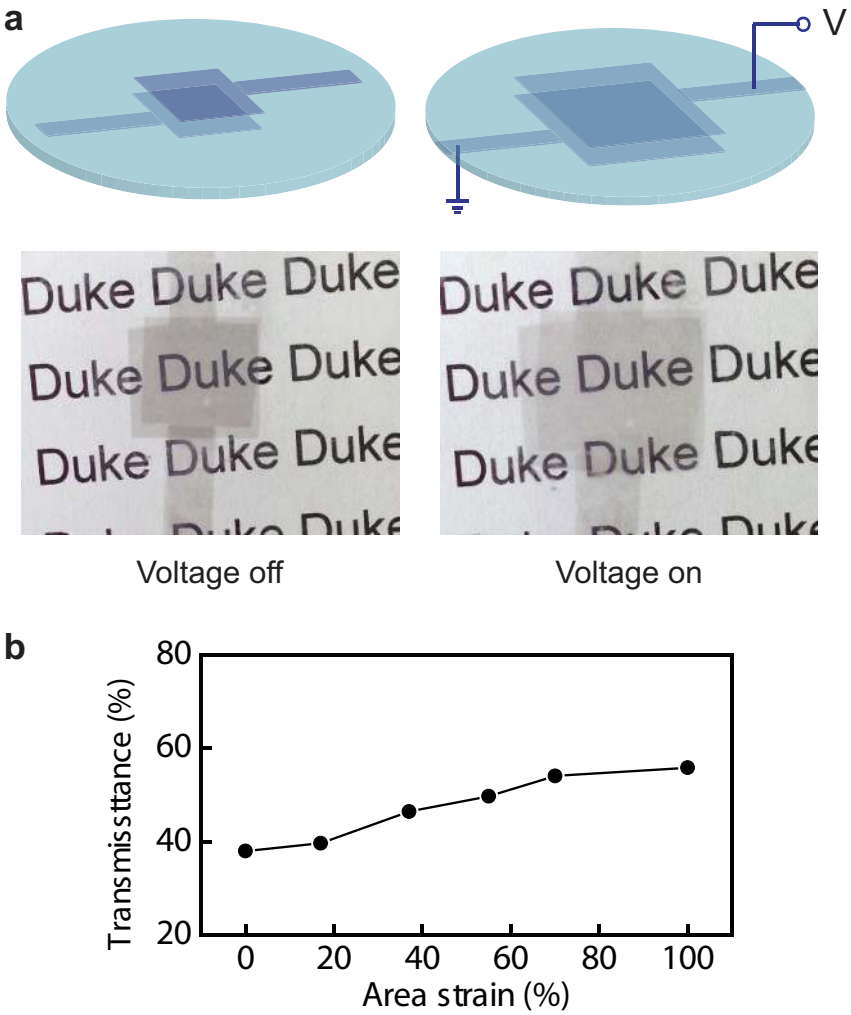

Fig 4. Voltage-induced actuation of a crumpled graphene-elastomer laminate. a, As a voltage is applied, the laminate reduces its thickness and expands its area. The area actuation strain is over 100%. **b,** Transmittance of the laminate in visible range as a function of the area actuation strain. Values in **b** represent mean of *n* tests ($n = 3$).